Supplementary Materials for

Tailoring Intersystem Crossing in Phosphorus-Corrole through Axial Chalcogenation: A Detailed Theoretical Study

Annette Mariya Tedy and Arun K Manna*

Department of Chemistry, Indian Institute of Technology Tirupati, Tirupati, A.P 517619, India

*Corresponding Author E-mail: arun@iittp.ac.in

Table of Contents:

Section A: Optimally Tuned Range-Separated Hybrid (OT-RSH)

For OT-RSH implementation, ωB97X-D RSH functional[1] is nonempirically and optimally tuned for each system to obtain an optimal range-separation parameter (ω^*) by minimizing the following error measure ($J^2(\omega)$)[2, 3] enforcing the ionization potential (IP) theorem:[4]

$$J^2(\omega) = \sum_{i=N}^{N+1} [IP^{\omega}\ (i) + E_H^{\omega}(i)]^2$$

Where, N is the number of electrons, and i = N, N+1 refers to neutral and anion systems respectively. $IP^{\omega}(i)$ and $E_H^{\omega}(i)$ are the ionization potential and the energy of HOMO of both neutral (i = N) and anion (i = N+1). The resultant RSH functional is customarily termed as the OT-RSH. Here we note that other parameters of the OT-ωB97X-D RSH (i.e., ω^*B97X-D) are kept fixed at their default values in the OT-RSH implementation. These default set of parameters like the amount of short-range Fock exchange (~22%) as present in ωB97X-D[1] have been shown to produce a robust and balanced description of both locally-excited (LE) and charge-transfer (CT) electronic states.[3]

We would like to emphasise that the optimal tuning is undertaken in the gas phase only, as the optimal tuning in PCM will lead to unphysically small ω values.[5] Although this caveat can be fixed by including dielectric screening in the RSH functional form itself,[6] this screened-RSH implementation is inevitable only for condensed-phase environments like thin-film/solids.[7-11] Moreover, the optimal ω tuned in the gas-phase can be translated to the solution phase, provided that there are only minimal orbital interactions between the solute and the solvent.[12] This is valid for the solvated systems in toluene studied in this work and the implicit solvation models like PCM adopted for accounting of the solvent effects. Importantly, OT-RSH has been shown to produce reliable and accurate description of both CT and LE states for a large variety of solvated molecules.[2, 3]

Section B: Ground-State Structural Properties of solvated PC and three X=PCs

In this section, we compare and contrast the ground-state geometries of all the studied X=PCs and PC that are fully optimized using dispersion corrected DFT in toluene (see Figure 1 from main article for all relaxed structures). The difluorophenyl meso-substituents are almost perpendicular to the macrocycle ring with calculated dihedral angles ranging from ~75° to ~81° in accordance with the previous literature findings reported for both FBC[13, 14] and other PC analogues.[15, 16] This essentially indicates limited orbitals contribution towards enhancing corrole π-conjugation by the meso-substituents. As shown in main article Figure 1, two different sets of N-P bond lengths are originated from the structural asymmetry created by the direct α - α pyrollic linkage of the corrole ring. Further, only a negligible increase in the N-P bond length is found in going from O to Se, suggesting minimal influence of the chalcogen on the corrole core structural properties. However, an increasing trend in the P=X bond length is found going from O to Se due to larger size of the chalcogen down the group. This is accompanied by a gradually increased ground-state electric dipole moment ($\mu = 4.0 - 4.7$ D) down the chalcogen-group, which is even larger than that in PC. An in-depth analysis reveals that μ of the P=X unit ($\mu_{P=X}$) is directed opposite to that of the corrole unit and thereby, partially reduces the corrole dipole. As a result, an increased μ of X=PC in going from X = O to Se is attributed to the decreased $\mu_{P=X}$, which is due to the smaller charge-separation as evident from the natural population analysis derived charges listed in Figure 1 of main article. The reduction in the partial charges down the chalcogen-group is due to the gradually decreased electronegativity of the associated X. On the other hand, much smaller charge on the central P in PC due to lower oxidation state results in comparatively lesser μ.

Section C: Ground and Excited States Electronic Structures of solvated PC and three X=PCs considered in this study

Electronic Structures at Ground-State Geometries: OT-RSH calculated low-lying FMOs are examined to explore and understand the ground-state electronic properties of the PC and X=PCs in toluene (see Figure S2 for FMOs iso-surfaces and their energies). Like porphyrin, corroles absorption bands also follow the celebrated Gouterman's four orbital model[17, 18] and therefore, we specifically looked at following four low-energy MOs: HOMO-1, HOMO for the occupied states and LUMO, LUMO+1 for the unoccupied states. All the studied X=PCs maintain the degeneracy of the HOMO and HOMO-1 orbitals as similar to the porphyrin analogues,[19, 20] whereas the orbital degeneracy is lifted in the case of LUMO and LUMO+1. On contrary, PC shows non-degenerate FMOs. The orbital picture found here for X=PCs is markedly different from the PCs and FBCs, where no such degeneracy was observed due to the symmetry-breaking. These results indicate that the oxidation of the central P by the chalcogens brought about a significant modification of the corrole electronic structures, which is reflected by a pair of near degenerate occupied and non-degenerate unoccupied orbitals. Such orbital degeneracy may have implications in the low-lying optical excitations of the X=PCs involving these FMOs as discussed in the main article text.

PC shows a HOMO-LUMO gap (ΔE_{H-L} hereafter) of ~4.8 eV. Among the four FMOs examined, the HOMO of PC acquires substantial P contribution (~25%), suggesting both macrocyclic-ring and P-centered oxidation. On the other hand, relatively larger ΔE_{H-L} of ~5.1-5.2 eV is found for its oxidized product X=PCs with much lowered P contribution to the FMOs. Further, it is also interesting to note that while the HOMO, HOMO-1 energies remain fairly constant among the studied X=PCs, the LUMO and LUMO+1 gets slightly stabilized by ~0.1 eV going from O to S. However, no appreciable change in the FMO energies is found between S=PC and Se=PC owing to the similar atomic radii and comparable electronic polarizabilities of S and Se. The ΔE_{H-L} also follows the same trend with a slight reduction going from O to S/Se. Overall, all three X=PCs show almost similar ΔE_{H-L} of ~5.1-5.2 eV. Like the analogous meso-substituted FBCs,[14] PC and X=PCs also exhibit π-type electron density in the corrole core with negligible contribution from the meso-substituents.

Interestingly, the HOMO-1 and HOMO of O=PC qualitatively resembles with the HOMO and HOMO-1, respectively of both S=PC and Se=PC. Although HOMO and HOMO-1 are almost degenerate for X=PCs, the contributions of the core N atoms towards these FMOs are markedly different (see Figure S2). The HOMO-1 of O=PC and HOMO of S=PC and Se=PC appear to possess larger N contribution. While calculated percentage of N contributions to these FMOs is ~13-16%, the HOMO of O=PC and HOMO-1 of S=PC and Se=PC acquire much smaller N contribution of ~4-6%. On the other hand, the percentage contribution of P ranges from 0.1 to 2.9% in the studied X=PC systems. Compared to this, parent PC shows P contribution ranging from ~0.2 to 24.5% and its biaxially fluorinated derivatives were shown to have only ~0.6% P contribution.[15] Varied extent of N and P contributions suggest that the core N may have more significance in improving the SOC via hetero-atom effect than the core P. Nevertheless, since P is heavier than N, even relatively smaller %P contribution may have more weightage than the N-contribution as SOC $\propto Z^4$, where Z is the atomic number of any hydrogen-like atoms. We note that both %P and %N towards the FMOs slightly improve going from O to Se. Qualitatively similar trend is also seen for the percentage contribution of the chalcogens as well. But, a significantly larger chalcogen contribution of ~18.7% is only found for HOMO-1 of Se=PC compared to other studied X=PC systems. Further, deeper lying HOMO-3 and HOMO-2 acquire relatively large chalcogen contributions (31-70%) for all three X=PCs with the largest contribution found for Se=PC (see Figure S3). Therefore, excited states involving transitions from HOMO-

3/HOMO-2/HOMO-1of Se=PC is expected to display larger SOC via virtue of the heavy-atom effect as discussed in the main article text.

Electronic Structures at the Excited-State Geometries: As discussed in the main article text, excited-state molecular geometries of PC and three X=PCs are slightly different from the ground-state ones (see ΔSCF and RMSD data from Figure S4). To examine the effect of excited-state nuclear reorganization on the electronic structure of the systems, we also analyse the FMOs at the respective optimized excited-state geometries as shown in SI Figure S5. It is interesting to note that at all of the excited-state geometries, the degeneracy of the HOMO-1 and HOMO is lifted for all the X=PCs. The ground-state electronic distribution (i.e., FMOs iso-surfaces) is qualitatively maintained at the excited-state geometries. But certain reordering between the HOMO-1 and HOMO is also seen due to the excited-state relaxation. For example, all the excited-state geometries of O=PC feature a HOMO that is similar to the HOMO-1 at the ground-state and a HOMO-1 similar to the ground-state HOMO (compare FMOs from SI Figure S2 and Figure S5). Similarly, HOMO-1 and HOMO of Se=PC at T_3 geometry resemble to HOMO and HOMO-1, respectively found at S_0 geometry. An improvement of the percentage chalcogen contribution to the FMOs is also seen at the excited-state geometries as compared to the ground-state for all the X=PCs. This is expected to impact the excited-state deactivation processes. Especially, since the ISC involves the equilibrium S_1 geometry the improved %chalcogen contribution found at this geometry may enhance the SOC for the ISC processes in the studied systems.

Table S1: Vertical (E^v) energy of the first few excited singlets (S_n) and a few low-lying triplet excited states (T_n) with dipole oscillator strength (OS) given in bracket, calculated using TD-OT-RSH at the solvated Franck-Condon geometry (S_0). Important occupied to unoccupied FMOs configurations (with major coefficients listed in bracket) at the S_0 geometry relevant to each excited-state are listed for solvated PC and three X=PCs in toluene. H and L represent HOMO and LUMO, respectively.

X=PC	Excited State (OS)	E^v (eV)	Contributions of FMOs
PC	S_1 (0.14)	1.98	H → L (0.67)
	S_2 (0.00)	2.32	H → L+1 (0.56); H-1 → L (0.42)
	S_3 (0.57)	2.78	H-1 → L (0.54); H → L+1 (0.39)
	S_4 (0.24)	3.01	H-1 → L+1 (0.61)

	S_5 (1.04)	3.64	H-2 → L (0.61)
	T_1	1.48	H → L (0.70)
	T_2	1.84	H-1 → L (0.65)
	T_3	1.92	H → L+1 (0.65)
	T_4	2.39	H-1 → L+1 (0.68)
O=PC	S_1 (0.11)	2.45	H-1 → L (0.58); H → L+1 (0.39)
	S_2 (0.08)	2.48	H → L (0.60); H-1 → L+1 (0.36)
	S_3 (1.42)	3.36	H → L+1 (0.58); H-1 → L (0.39)
	S_4 (1.22)	3.40	H-1 → L+1 (0.60); H → L (0.36)
	T_1	1.88	H-1 → L (0.65)
	T_2	1.89	H → L (0.67)
	T_3	2.31	H-1 → L+1 (0.68)
	T_4	2.42	H → L+1 (0.67)
	T_5	3.64	H-3 → L (0.62)
	T_6	3.66	H-2 → L (0.62)
S=PC	S_1 (0.11)	2.39	H → L (0.59); H-1 → L+1 (0.38)
	S_2 (0.06)	2.42	H-1 → L (0.60); H → L+1 (0.36)
	S_3 (0.01)	2.80	H-2 → L (0.69)
	S_4 (0.01)	2.86	H-3 → L (0.67)
	S_5 (0.35)	3.15	H-3 → L+1 (0.50); H-1 → L+1 (0.42)
	S_6 (0.76)	3.30	H → L+1 (0.46); H-2 → L+1 (0.39); H-1 → L (0.33)
	S_7 (0.37)	3.32	H-2 → L+1 (0.56); H → L+1 (0.33)
	S_8 (0.92)	3.37	H-3 → L+1 (0.48); H-1 → L+1 (0.41)
	T_1	1.83	H → L (0.68)
	T_2	1.87	H-1 → L (0.69)
	T_3	2.23	H → L+1 (0.69)
	T_4	2.37	H-1 → L+1 (0.68)
	T_5	2.75	H-3 → L (0.54); H-2 → L (0.44)
	T_6	2.75	H-2 → L (0.54); H-3 → L (0.44)
Se=PC	S_1 (0.04)	2.34	H-1 → L (0.60)
	S_2 (0.11)	2.36	H → L (0.58); H-1 → L+1 (0.35)
	S_3 (0.00)	2.41	H-2 → L (0.69)
	S_4 (0.01)	2.54	H-3 → L (0.62)

	S_5 (0.03)	2.80	H-3 → L+1 (0.57); H-1 → L+1 (0.39)
	S_6 (0.02)	2.92	H-2 → L+1 (0.69)
	S_7 (1.06)	3.27	H → L+1 (0.56); H-1 → L (0.33)
	S_8 (1.17)	3.29	H-1 → L+1 (0.46); H-3 → L+1 (0.38); H → L (0.35)
	T_1	1.80	H → L (0.68)
	T_2	1.86	H-1 → L (0.67)
	T_3	2.20	H → L+1 (0.65)
	T_4	2.35	H-1 → L+1 (0.65)
	T_5	2.38	H-2 → L (0.66)
	T_6	2.39	H-3 → L (0.63)
	T_7	2.76	H-2 → L+1 (0.69)

Table S2: OT-RSH calculated vertical (E^{v}), adiabatic (E^{ad}) and 0-0 (E^{0-0}) energies of S_1 and relevant T_n states near or below S_1 for the studied PC and X=PC systems in toluene.

X=PC	States	S_1	T_1	T_2	T_3	T_4	T_5	T_6
PC	E^{v} (eV)	1.98	1.48	1.84	1.92	-	-	-
	E^{ad} (eV)	1.56	1.33	1.73	1.77	-	-	-
	E^{0-0} (eV)	1.56	1.28	1.75	1.72	-	-	-
O=PC	E^{v} (eV)	2.45	1.88	1.89	2.31	2.42	-	-
	E^{ad} (eV)	2.41	1.73	1.74	2.01	2.12	-	-
	E^{0-0} (eV)	2.34	1.63	1.64	1.91	2.02	-	-
S=PC	E^{v} (eV)	2.39	1.83	1.87	2.23	2.37	-	-
	E^{ad} (eV)	2.35	1.68	1.72	1.93	2.07	-	-
	E^{0-0} (eV)	2.28	1.58	1.62	1.83	1.97	-	-
Se=PC	E^{v} (eV)	2.34	1.80	1.86	2.20	2.35	2.38	2.39
	E^{ad} (eV)	2.30	1.65	1.71	1.90	2.05	1.98	1.99
	E^{0-0} (eV)	2.24	1.56	1.62	1.80	1.95	1.88	1.89

Table S3: Calculated ΔE_{S-T}, SOC and k_{ISC} for $S_1 \rightarrow T_n$ ISC processes for PC and X=PCs in toluene. $\Delta E_{S-T} = E(S_1) - E(T_n)$ based on 0-0 energies and a positive ΔE_{S-T} refers to T_n below to S_1.

$S_1 \rightarrow T_n$	PC	O=PC

	ΔE_{S-T} (eV)	SOC (cm^{-1})	k_{ISC} (s^{-1})	ΔE_{S-T} (eV)	SOC (cm^{-1})	k_{ISC} (s^{-1})
$S_1 \rightarrow T_1$	0.28	0.18	1.28×10^{7}	0.71	0.16	2.75×10^{3}
$S_1 \rightarrow T_2$	-0.19	0.99	1.83×10^{5}	0.70	0.89	1.08×10^{5}
$S_1 \rightarrow T_3$	-0.16	1.90	3.42×10^{6}	0.43	0.75	3.21×10^{7}
$S_1 \rightarrow T_4$	-	-	-	0.32	0.06	1.01×10^{6}
$S_1 \rightarrow T_n$	S=PC			Se=PC		
	ΔE_{S-T} (eV)	SOC (cm^{-1})	k_{ISC} (s^{-1})	ΔE_{S-T} (eV)	SOC (cm^{-1})	k_{ISC} (s^{-1})
$S_1 \rightarrow T_1$	0.70	2.45	9.88×10^{5}	0.68	135.68	4.29×10^{9}
$S_1 \rightarrow T_2$	0.66	3.28	4.43×10^{6}	0.62	42.51	1.66×10^{9}
$S_1 \rightarrow T_3$	0.45	3.28	9.11×10^{8}	0.43	68.58	3.97×10^{11}
$S_1 \rightarrow T_4$	0.31	0.56	8.60×10^{7}	0.36	367.46	2.56×10^{13}
$S_1 \rightarrow T_5$	-	-	-	0.35	494.25	5.06×10^{13}
$S_1 \rightarrow T_6$	-	-	-	0.29	110.87	4.22×10^{12}

Table S4: Calculated effective Huang-Rhys factor (S_{eff}) and effective high-frequency vibrational mode ($< \omega_{eff} >$, in cm^{-1}) for relevant $S_1 \rightarrow T_n$ ISC processes for solvated PC and X=PCs in toluene.

X=PC	PC		O=PC		S=PC		Se=PC	
	S_{eff}	$< \omega_{eff} >$	S_{eff}	$< \omega_{eff} >$	S_{eff}	$< \omega_{eff} >$	S_{eff}	$< \omega_{eff} >$
$S_1 \rightarrow T_1$	0.1023	1662	0.0280	1590	0.0322	1593	0.0293	1593
$S_1 \rightarrow T_2$	0.6306	1500	0.0280	1590	0.0322	1593	0.0293	1593
$S_1 \rightarrow T_3$	0.1023	1662	0.0594	1646	0.3413	1630	0.2365	1455
$S_1 \rightarrow T_4$	-	-	0.0594	1646	0.3413	1630	0.3679	1379
$S_1 \rightarrow T_5$	-	-	-	-	-	-	0.3679	1379
$S_1 \rightarrow T_6$	-	-	-	-	-	-	0.2365	1455

Table S5: Calculated fluorescence rate constants (k_F) and phosphorescence rate constant (k_P) from the relaxed bright S_n and T_n ($n = 1{,}2$), respectively for solvated PC and X=PCs in toluene. S_n/T_n vertical emission energies with dipole oscillator strength (values within bracket) calculated at the respective optimized solvated optically bright S_n and T_1 geometries for each of the X=PCs are also listed.

Systems	S_1 (eV)	k_F (s^{-1})	S_3 (eV)	k_F (s^{-1})	T_1 (eV)	k_P (s^{-1})	T_2 (eV)	k_P (s^{-1})
PC	0.97 (0.03)	1.34 × 10^6	-	-	1.19 (3.14 × 10^{-7})	34.8	-	-
O=PC	2.38 (0.17)	9.09 × 10^7	3.24 (1.47)	1.45 × 10^9	1.61 (1.31 × 10^{-8})	2.83	1.91 (3.32 × 10^{-8})	11.9
S=PC	2.31 (0.17)	8.52 × 10^7	-	-	1.57 (3.53 × 10^{-7})	72.5	1.89 (6.99 × 10^{-7})	2.45 × 10^2
Se=PC	2.28 (0.15)	7.38 × 10^7	-	-	1.55 (1.69 × 10^{-4})	3.40 × 10^4	1.88 (1.92 × 10^{-4})	6.65 × 10^4

Table S6: 0-0 corrected T_n $(n = 1,2)$ energies and OT-RSH calculated SOC and k_{nr} for $T_n \rightarrow S_0$ $(n = 1, 2)$ ISC processes at solvated optimized T_1 geometry for solvated PC and three X=PCs in toluene.

$T_n \rightarrow S_0$	PC			O=PC		
	T_n (eV)	SOC (cm^{-1})	k_{nr} (s^{-1})	T_n (eV)	SOC (cm^{-1})	k_{nr} (s^{-1})
$T_1 \rightarrow S_0$	1.28	1.89	4.02 × 10^2	1.63	0.29	2.22 × 10^{-1}
$T_2 \rightarrow S_0$	-	-	-	1.64	0.21	9.87 × 10^{-2}
$T_n \rightarrow S_0$	S=PC			Se=PC		
	T_n (eV)	SOC (cm^{-1})	k_{nr} (s^{-1})	T_n (eV)	SOC (cm^{-1})	k_{nr} (s^{-1})
$T_1 \rightarrow S_0$	1.58	2.57	59.95	1.56	18.34	1.74 × 10^3
$T_2 \rightarrow S_0$	1.62	1.08	5.56	1.62	7.77	1.19 × 10^2

Table S7: Calculated triplet lifetimes (τ_T) for T_n $(n = 1, 2)$ states at the optimized T_1 geometry for the studied PC and X=PCs in toluene.

System	T_1		T_2	
	$k_P + k_{nr}$ (s^{-1})	τ_T (s)	$k_P + k_{nr}$ (s^{-1})	τ_T (s)
PC	4.37 × 10^2	2.29 × 10^{-3}	-	-
O=PC	3.05	3.28 × 10^{-1}	12.00	8.33 × 10^{-2}
S=PC	1.32 × 10^2	7.55 × 10^{-3}	2.51 × 10^2	3.99 × 10^{-3}
Se=PC	3.57 × 10^4	2.80 × 10^{-5}	6.66 × 10^4	1.50 × 10^{-5}

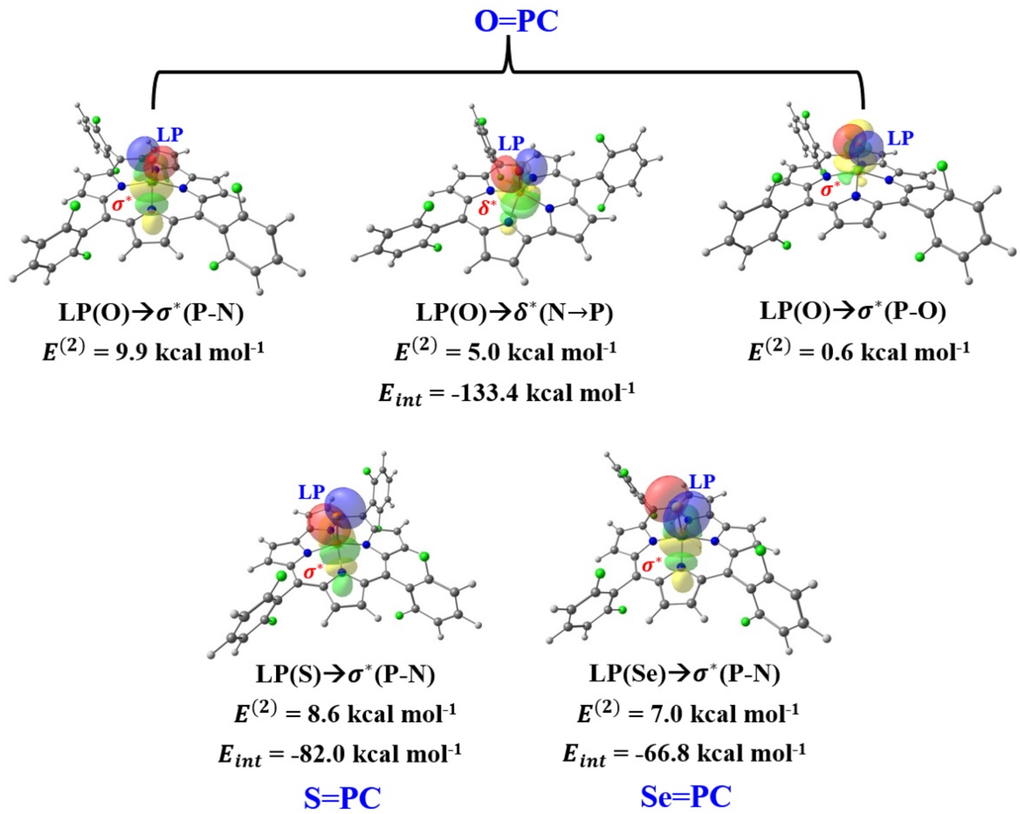

Figure S1: Natural bond orbitals displaying the donor-acceptor orbital interaction between the lone-pair (LP) of chalcogen (X) and different non-bonding orbitals (σ^*, δ^*), where σ and δ refer to the sigma and dative bond, respectively. An iso-value of 0.05 electrons/bohr^3 is used for the iso-surfaces. Calculated second-order perturbation energy ($E^{(2)}$) and interaction energy (E_{int}) between the X and PC are also listed.

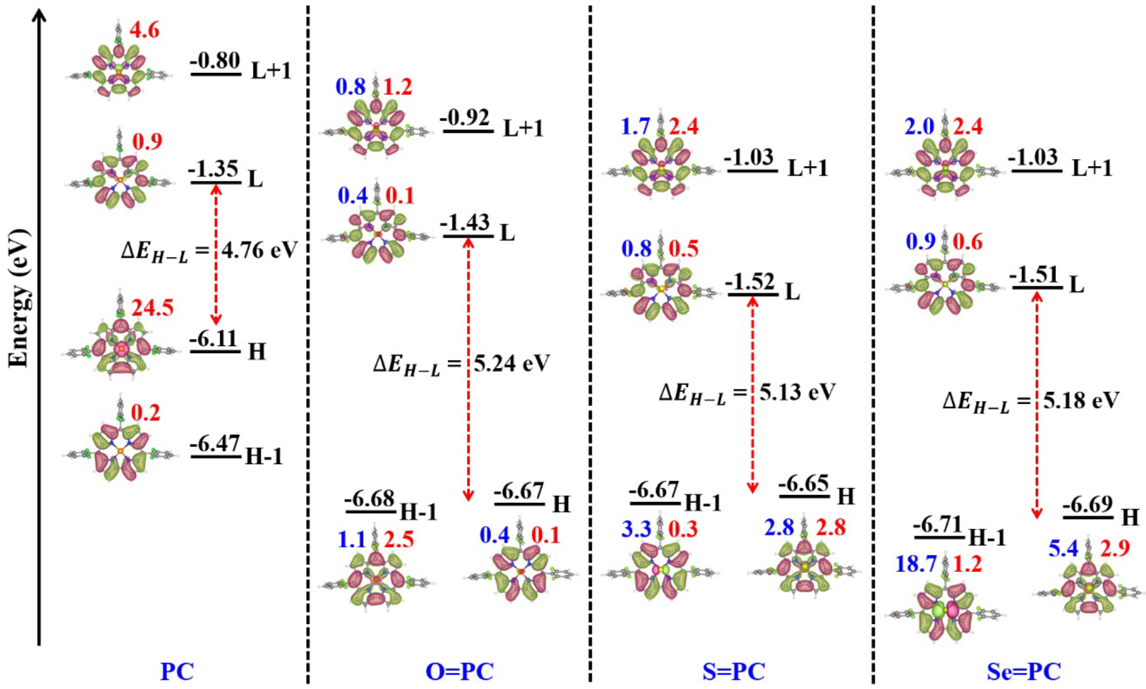

Figure S2: OT-RSH calculated FMO energies and iso-surfaces of the studied PC and X=PCs in toluene. HOMO (H-1), HOMO (H), LUMO (L), and LUMO+1 (L+1) are shown along with the HOMO-LUMO gap (ΔE_{H-L}) and percentage contributions of P (in red colour numbers) and chalcogen (in blue colour numbers) towards the FMOs. An iso-value of 0.02 electrons/bohr^3 is used for the iso-surfaces.

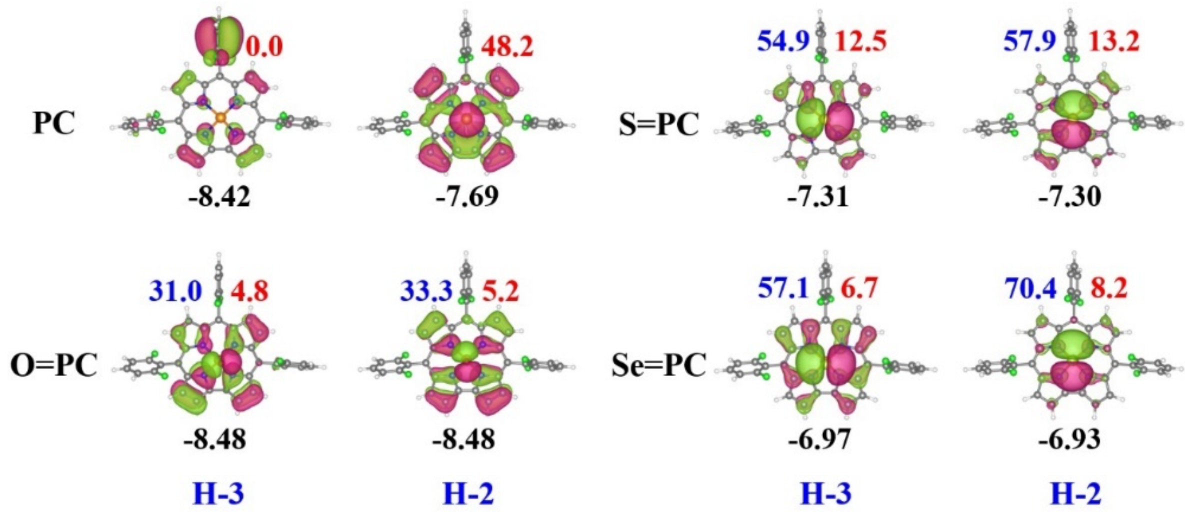

Figure S3: OT-RSH calculated energies and iso-surfaces of HOMO-3 and HOMO-2 for the studied systems in toluene. H stands for HOMO. Percentage contributions of P (in red colour numbers) and chalcogen (in blue colour numbers) towards the FMOs are also shown. An iso-value of 0.02 electrons/bohr^3 is used for the iso-surfaces. All energies are in eV.

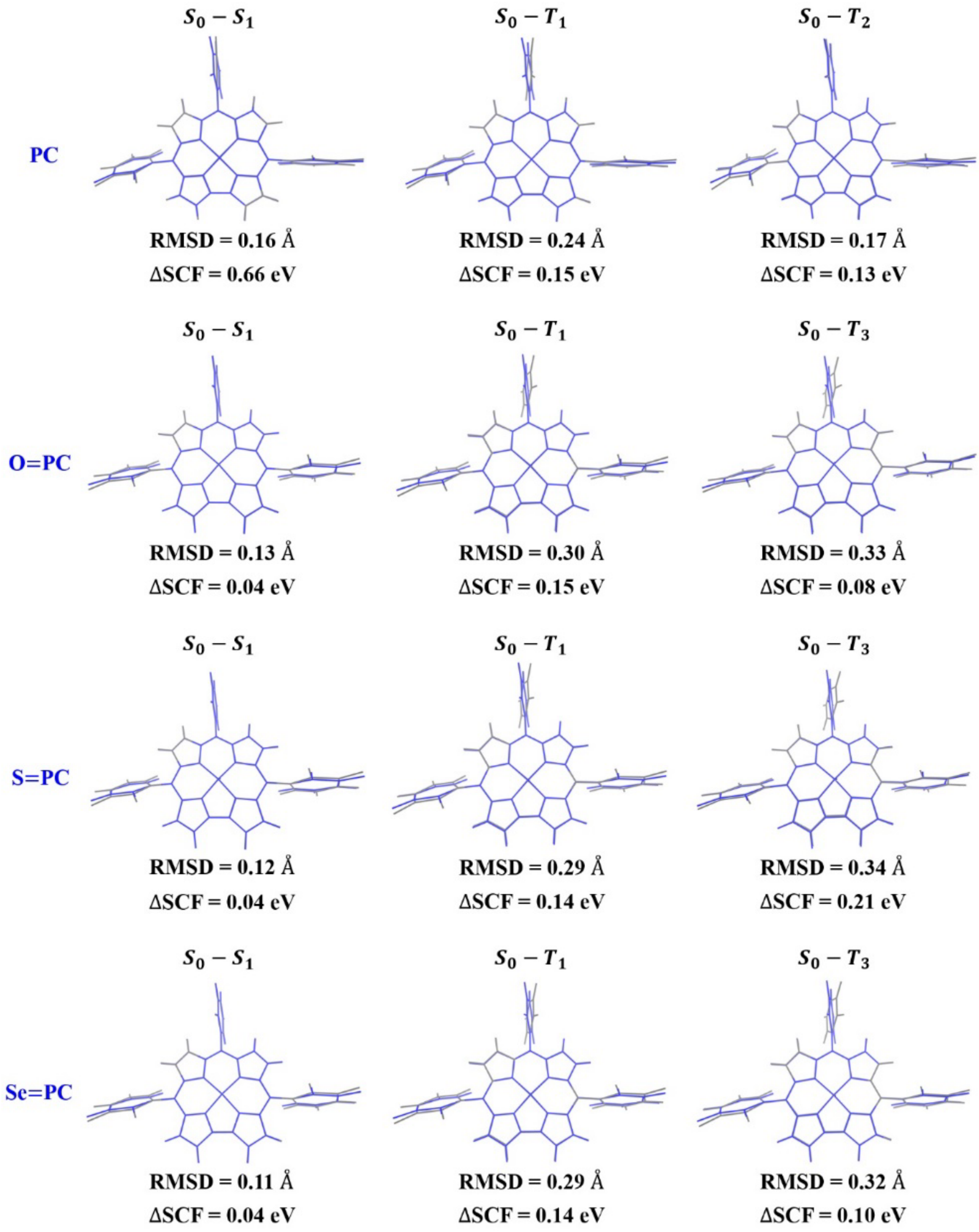

Figure S4: Calculated RMSD and ΔSCF energy differences between the ground-state and the relevant excited-state geometries. Blue- and grey-colour represent the ground-state (S_0) and the relevant excited-state (S_1 or T_n) geometries.

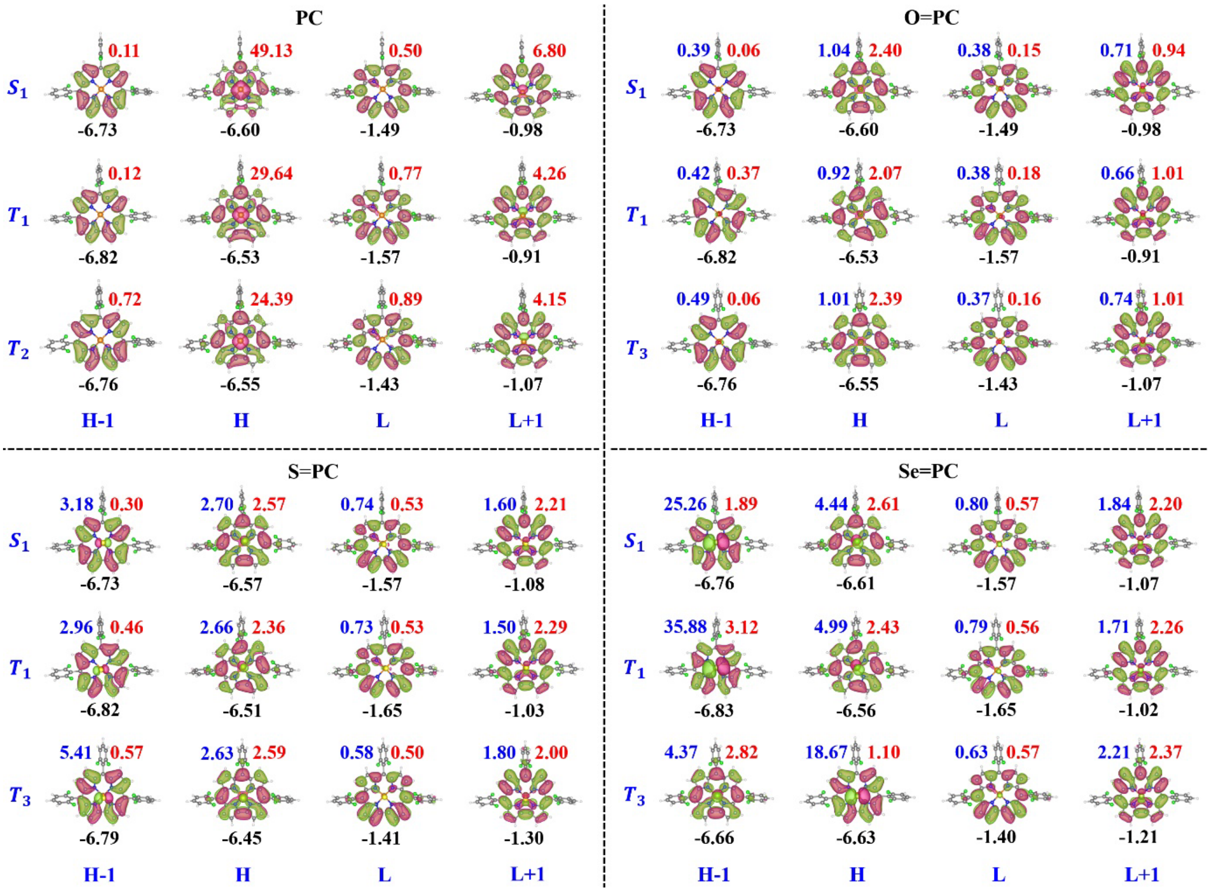

Figure S5: OT-RSH calculated FMOs iso-surfaces and energies at the respective excited-state geometries of the studied X=PC systems in toluene. H and L stand for the HOMO and LUMO, respectively. Percentage contributions of P and chalcogen toward the FMOs are listed in red- and blue-coloured numbers, respectively. An iso-value of 0.02 electrons/Bohr^3 is used for the iso-surface plot.

References:

1. J.-D. Chai and M. Head-Gordon, Long-range corrected hybrid density functionals with damped atom-atom dispersion corrections, *Phys. Chem. Chem. Phys.,* 2008, **10**, 6615-6620.
2. T. Stein, L. Kronik and R. Baer, Prediction of charge-transfer excitations in coumarin-based dyes using a range-separated functional tuned from first principles, *J. Chem. Phys.,* 2009, **131**, 244119.
3. L. Kronik, T. Stein, S. Refaely-Abramson and R. Baer, Excitation gaps of finitesized systems from optimally tuned range-separated hybrid functionals, *J. Chem. Theory Comput.,* 2012, **8**, 1515-1531.

4. J. F. Janak, Proof that $\frac{\delta E}{\delta n_i} = \varepsilon_i$ in density-functional theory, *Phys. Rev. B,* 1978, **18**, 7165-7168.
5. T. B. de Queiroz and S. Kümmel, Charge-transfer excitations in low-gap systems under the influence of solvation and conformational disorder: Exploring range-separation tuning, *J. Chem. Phys.,* 2014, **141**, 084303-084312.
6. L. Kronik and S. Kümmel, Dielectric screening meets optimally tuned density functionals, *Adv. Mater.,* 2018, **30**, 1706560.
7. S. Bhandari, M. S. Cheung, E. Geva, L. Kronik and B. D. Dunietz, Fundamental gaps of condensed-phase organic semiconductors from single-molecule calculations using polarization-consistent optimally tuned screened range-separated hybrid functionals, *J. Chem. Theory Comput.,* 2018, **14**, 6287-6294.
8. S. Bhandari and B. D. Dunietz, Quantitative accuracy in calculating charge transfer state energies in solvated molecular complexes using a screened range separated hybrid functional within a polarized continuum model, *J. Chem. Theory Comput*., 2019, **15**, 4305-4311.
9. A. K. Manna, S. Refaely-Abramson, A. M. Reilly, A. Tkatchenko, J. B. Neaton and L. Kronik, Quantitative prediction of optical absorption in molecular solids from an optimally tuned screened range-separated hybrid functional, *J. Chem. Theory Comput.,* 2018, **14**, 2919-2929.
10. R. Ahmed and A. K. Manna, Origins of large Stokes shifts in a pyrene–styrene based push–pull organic molecular dyad in polar solvents and large electron mobility in the crystalline state: A theoretical perspective, *J. Phys. Chem. C,* 2022, **126**, 423-433.
11. Z. Zheng, D. A. Egger, J.-L. Brédas, L. Kronik and V. Coropceanu, Effect of solid-state polarization on charge-transfer excitations and transport levels at organic interfaces from a screened range-separated hybrid functional, *J. Phys. Chem. Lett.,* 2017, **8**, 3277-3283.
12. T. B. de Queiroz and S. Kümmel, Tuned range separated hybrid functionals for solvated low bandgap oligomers, *J. Chem. Phys*., 2015, **143**, 034101.
13. J. F. B. Barata, G. P. M. S. Neves, M. A. F. Faustino, A. C. Tomé and J. A. S. Cavaleiro, Strategies for Corrole Functionalization, *Chem. Rev.,* 2017, **117**, 3192-3253.

14. A. M. Tedy, R. Ahmed and A. K. Manna, Assessing Intersystem Crossing Rates in Donor- and/Acceptor-Functionalized Corroles: A Computational Study, *J. Phys. Chem. A,* 2023, **127**, 3347-3355.

15. A. M. Tedy and A. K. Manna, Does the Intersystem Crossing Rate of β-Iodinated Phosphorus Corrole Depend on Iodine Numbers and/or Positions?, *J. Phys. Chem. A,* **2023,** ***127***, 10118-1012.

16. A. Mahammed, K. Chen, J. Vestfrid, J. Zhao and Z. Gross, Phosphorus corrole complexes: from property tuning to applications in photocatalysis and triplet-triplet annihilation upconversion, *Chem. Sci.,* 2019, **10**, 7091-7103.

17. N. S. Hush, J. M. Dyke, M. L. Williams and I. S. Woolsey, Electronic spectra of metal corrole anions, *J. Chem. Soc., Dalton Trans.,* 1974, 395-399.

18. A. Ghosh, T. Wondimagegn and A. B. J. Parusel, Electronic Structure of Gallium, Copper, and Nickel Complexes of Corrole. High-Valent Transition Metal Centers versus Noninnocent Ligands, *J. Am. Chem. Soc.,* 2000, **122**, 5100-5104.

19. M. Gouterman, Spectra of porphyrins, *J. Mol. Spectrosc.,* 1961, **6**, 138-163.

20. M. Gouterman, G. H. Wagniére and L. C. Snyder, Spectra of Porphyrins. Part II. Four-Orbital Model, *J. Mol. Spectrosc.,* 1963, **11**, 108-115.